Long Stephen (Orcid ID: 0000-0002-8501-7164)
Whitney Spencer (Orcid ID: 0000-0003-2954-2359)

BSD2 is a Rubisco specific assembly chaperone, forms intermediary hetero-oligomeric complexes and is non-limiting to growth in tobacco.

Running title: The content, function and necessity of BSD2 in plants

Brendon Conlan[1], Rosemary Birch[1], Celine Kelso[2], Sophie Holland[1], Amanda P. De Souza[3], Stephen P Long[3,4], Jennifer L. Beck[2], Spencer M. Whitney[1*]

[1]Research School of Biology, The Australian National University, Acton, Australian Capital Territory 2601, Australia. [2]School of Chemistry, Molecular Horizons, University of Wollongong, New South Wales 2522, Australia. [3]Carl R. Woese Institute for Genomic Biology, University of Illinois, Urbana, Illinois 61801, USA. [4]Lancaster Environment Centre, Lancaster University, Lancaster LA1 4YQ, UK.

*Corresponding author: Research School of Biology, 134 Linnaeus Way, The Australian National University, Acton, Australian Capital Territory 0200, Australia; T: +61-2-6125-5073; E: spencer.whitney@anu.edu.au

This is the author manuscript accepted for publication and has undergone full peer review but has not been through the copyediting, typesetting, pagination and proofreading process, which may lead to differences between this version and the Version of Record. Please cite this article as doi: 10.1111/pce.13473

Abstract

The folding and assembly of Rubisco large and small subunits into L_8S_8 holoenzyme in chloroplasts involves many auxiliary factors, including the chaperone BSD2. Here we identify apparent intermediary Rubisco-BSD2 assembly complexes in the model C_3-plant tobacco. We show BSD2 and Rubisco content decrease in tandem with leaf age with approximately half of the BSD2 in young leaves (~70 nmol BSD2 protomer.m^2) stably integrated in putative intermediary Rubisco complexes that account for <0.2% of the L_8S_8 pool. RNAi-silencing BSD2 production in transplastomic tobacco producing bacterial L_2 Rubisco had no effect on leaf photosynthesis, cell ultrastructure or plant growth. Genetic crossing the same RNAi-*bsd2* alleles into wild-type tobacco however impaired L_8S_8 Rubisco production and plant growth, indicating the only critical function of BSD2 is in Rubisco biogenesis. Agrobacterium mediated transient expression of tobacco, Arabidopsis or maize BSD2 re-instated Rubisco biogenesis in BSD2-silenced tobacco. Overexpressing BSD2 in tobacco chloroplasts however did not alter Rubisco content, activation status, leaf photosynthesis rate or plant growth in the field or in the glasshouse at 20°C or 35°C. Our findings indicate BSD2 functions exclusively in Rubisco biogenesis, can efficiently facilitate heterologous plant Rubisco assembly and is produced in amounts non-limiting to tobacco growth.

Keyword index: photosynthesis, chaperone, protein folding, RuBP carboxylation

Introduction:

The content and kinetic properties of the CO_2-fixing enzyme Rubisco strongly influence the photosynthetic carbon fixation rate and resource use efficiency of vascular plants (Carmo-Silva, Scales, Madgwick & Parry, 2015). As a consequence of its slow turnover rate, low affinity for CO_2 and competitive inhibition by O_2 the resource allocation into Rubisco by crops such as rice and wheat is vast – Rubisco comprising up to 50% of the leaf soluble protein and 30% of leaf nitrogen (Evans & Seemann, 1989, Makino, 2003). Improving the carboxylation kinetics of Rubisco is therefore predicted to beneficially impact crop resource use, growth and yield (Long, Marshall-Colon & Zhu, 2015).

Structure-function studies over the last 5 decades have identified extensive natural diversity in the subunit stoichiometry and carboxylation kinetics among the Rubisco superfamily (Sharwood, 2017). Marked differences have also been uncovered in the folding and assembly requirements of the Rubisco ~50kDa large (L) subunits that form either homo-oligomeric L_2 to L_{10} complexes (Form II and III Rubisco) or form L_8 cores that bind eight small (S) subunits (~15 kDa) to stabilise and initiate L_8S_8 Form I Rubisco activity (Bracher, Whitney, Hartl & Hayer-Hartl, 2017). The biogenesis and metabolic maintenance of plant L_8S_8 Rubisco within the stroma of chloroplasts appears to require extensive accessory protein interactions (Conlan & Whitney, 2018, Wilson & Hayer-Hartl, 2018), whose structural complementarity with Rubisco can dramatically influence its assembly and activity regulation (Durao, Aigner, Nagy, Mueller-Cajar, Hartl & Hayer-Hartl, 2015, Whitney, Birch, Kelso, Beck & Kapralov, 2015). For research purposes this need for structural complementarity has limited the potential to express plant Rubisco in prokaryotic systems and in the chloroplasts

of a heterologous plant species (Sharwood, 2017). The need for Rubisco to preserve structural complementarity with its accessory proteins also appears to have influenced its catalytic evolution (Aigner, Wilson, Bracher, Calisse, Bhat, Hartl & Hayer-Hartl, 2017, Mueller-Cajar & Whitney, 2008, Wilson & Hayer-Hartl, 2018).

Bioengineering Rubisco in tobacco chloroplasts via plastome transformation has proven a useful synthetic biology tool to expose, and evaluate, variations in the enzymes biogenesis requirements between species (Sharwood, 2017). For example, the folding and assembly requirements of L_8S_8 Rubisco from cyanobacteria, non-green microalgae and monocot grasses are either poorly compatible (Lin, Occhialini, Andralojc, Parry & Hanson, 2014, Long, Hee, Sharwood, Rae, Kaines, Lim, Nguyen, Massey, Bala, von Caemmerer, Badger & Price, 2018, Wilson, Martin-Avila, Conlan & Whitney, 2018) or incompatible (Sharwood, Ghannoum, Kapralov, Gunn & Whitney, 2016, Whitney, Baldet, Hudson & Andrews, 2001) with the protein assembly machinery of tobacco chloroplasts. By contrast the simple assembly requirements of *R. rubrum* Form II Rubisco allow for near wild-type amounts of this faster, but low CO_2-affinity, L_2 Rubisco to be expressed in tobacco leaves (Wilson, Alonso & Whitney, 2016). Understanding the biochemical foundation for this diversity in expression potential has gradually advanced over the last decade through sequential discovery of the cellular components needed for Rubisco assembly and activity (Bracher *et al.*, 2017, Wilson & Hayer-Hartl, 2018). These studies recently culminated in the demonstration that active *Arabidopsis thaliana* L_8S_8 Rubisco could be reconstituted in *E. coli* when co-expressed with a cocktail of cognate chloroplast protein folding machinery components (Aigner *et al.*, 2017). These components included the differing subunits of the

chloroplast macromolecular chaperonin folding machinery (CPN60β, CPN60α, CPN21) and the structurally unrelated Rubisco assembly chaperones Rubisco accumulating factor 1 and 2 (Raf1, Raf2), bundle sheath defective 2 protein (BSD2) and RbcX.

Production of the ~40 kDa Raf1 chaperone is critical, and functionally specific, to plant Rubisco production (Feiz, Williams-Carrier, Wostrikoff, Belcher, Barkan & Stern, 2012, Hauser, Bhat, Milicic, Wendler, Hartl, Bracher & Hayer-Hartl, 2015). Structural complementarity between the L-subunits and Raf1 homodimers is required for optimal post-chaperonin stabilisation of antiparallel L_2 units which can assemble into $(L_2\text{-Raf1})_4$ intermediary complexes. Exploiting the Raf1 complementarity need has benefited efforts to introduce foreign Rubiscos into leaf chloroplasts by plastome transformation (Whitney *et al.*, 2015). Comparable to Raf1, the ~15 kDa RbcX is a homodimer and a Rubisco specific chaperone that can also form $L_8(RbcX_2)_8$ intermediary complexes (Liu, Young, Starling-Windhof, Bracher, Saschenbrecker, Rao, Rao, Berninghausen, Mielke, Hartl, Beckmann & Hayer-Hartl, 2010). The efficiency of L_8S_8 production is also influenced by sequence compatibility between the L-subunit C-terminus and RbcX homodimers (Durao *et al.*, 2015, Emlyn-Jones, Woodger, Price & Whitney, 2006). While Raf1 is crucial for Rubisco biogenesis, RbcX is not critical for recombinant plant Rubisco expression in *E. coli* (Aigner *et al.*, 2017) and provides no benefit to cyanobacteria L_8S_8 Rubisco expression in tobacco plastids (Lin *et al.*, 2014), is not required for Rubisco production in some cyanobacteria (Emlyn-Jones *et al.*, 2006) and a Rubisco assembly role *in planta* remains ambiguous. Questions also remain as to the multi-functional role of the ~19 kDa Raf2 chaperone within the chloroplast and other cellular locations. Deleting Raf2 in maize and *A. thaliana* almost

fully impairs Rubisco production (Feiz, Williams-Carrier, Belcher, Montano, Barkan & Stern, 2014, Rikard, Chen, Nicole, M., M., Linda, Jeremy, M., S., Todd & Roberta, 2018) in agreement with *A. thaliana* Rubisco production in *E. coli* being reliant on Raf2 expression (Aigner *et al.*, 2017). Additional roles for Raf2 in the cytosol and nucleus are associated with hormone and stress signalling and it has been found to be a target for viral infection (Oh, Kim, Cho, Ryu, Yang & Kim, 2017, Sun, Li, Wang, Zhao, Zhao, Zhang, Li, Yu, Wang, Zhang & Han, 2018). Resolving the structure and function(s) of Raf2 in plants poses one of the remaining challenges for mechanistically understanding the core Rubisco biogenesis process in plant chloroplasts.

It has been known for two decades that plant viability is dependent on the production of the ~8kDa, chloroplast located, BSD2 zinc-finger protein (Brutnell, Sawers, Mant & Langdale, 1999). It was proposed this dependency stems from the critical chaperone role BSD2 plays in Rubisco assembly in plants and green algae. Other functions proposed for BSD2 in cellular metabolism include regulating *rbc*L translation via interactions with nascent L-subunits (Doron, Segal, Gibori & Shapira, 2014) as well as influencing chloroplast coverage in the bundle sheath cells of maize (a C_4-plant) where Rubisco is located (Salesse, Sharwood, Sakamoto & Stern, 2017). Recent success in deriving the structural and mechanistic detail for BSD2 showed it forms an elongated, crescent shaped monomer with four cysteines that co-ordinate with two Zn atoms forming a hairpin structure that can displace other assembly chaperones and bind to L_8 cores producing stable $L_8(BSD2)_8$ intermediary complexes (Aigner *et al.*, 2017). It is proposed passive or assisted binding of S-

subunits to this end-state assembly intermediate facilitates BSD2 displacement to allow L_8S_8 holoenzyme formation.

In this study we examine the content and mechanistic properties of BSD2 *in situ* in tobacco, evaluate its Rubisco chaperone function and appraise its importance in the context of synthetic biology objectives for transplanting more efficient Rubisco isoforms into crops. Using an array of nuclear and plastome transformation approaches we demonstrate the chaperone function of BSD2 is Form I Rubisco specific, and can efficiently assemble heterologous plant L-subunits via the formation of stable, recognisable L_8-BSD2 intermediary complexes in plants. Our findings indicate BSD2 is naturally produced in amounts that are non-limiting to photosynthesis and growth in the model C_3-plant tobacco, even when grown in the glass house under non-optimal temperatures (20°C or 35°C) or in the field under un-regulated temperature and natural illumination.

Methods

Transient expression, nuclear and plastome transformation.

Nuclear transformed tobRr$^{\Delta B2}$ genotypes with *bsd2* expression knocked down in the tobacco genotype tobRr (also called ^{cm}trL, Fig 2A, (Whitney & Sharwood, 2008)), were generated by Agrobacterium (GV3101) transformation using the RNAi-*bsd2* binary vectors ptobRNAi-B2*k* or ptobRNAi-B2*b* (Fig 3A,B). Details of the RNAi-*bsd2* sequence are shown in Fig S3A. Homozygous, single insertion *k1*, *k2* and *b1* tobRr$^{\Delta B2}$ lines were identified by antibiotic segregation (Fig S4). Heterozygous tob$^{\Delta B2}$ progeny (where *bsd2* expression is knocked down

in wildtype tobacco) were generated by fertilising wild-type tobacco flowers with pollen from each homozygous tobRr$^{\Delta B2}$ *k1*, *k2* and *b1* line (Fig 4A).

Transient BSD2 expression was tested in tob$^{\Delta B2}$*b1* via Agrobacterium (GV3101) infiltration (Fig 5A). Synthetic tobacco, Arabidopsis and maize *bsd2* genes (codon use matching tobacco *rbcL*) which would not be silenced by the nuclear RNAi-*bsd2* allele were ordered from Genscript and cloned into the binary vector pBIN19 (Fig 3A).

The chloroplast transforming plasmid pRVB2 (Genbank Accession number pending, Fig 6A) was stably transformed into the tobacco plastome by biolistic transformation as described previously (Svab & Maliga, 1993). Two of the 6 transplastomic tobB2 lines obtained from 5 leaf bombardments were propagated to homoplasmicity via three successive rounds of selection on spectinomycin (0.5g.mL^{-1}). Both lines grew to reproductive maturity with the flowers of the T_0 and T_1 plants cross fertilised with wild-type tobacco pollen to attenuate any accompanying nuclear transgenic event.

Plant tissue culture, growth chamber and field growth.

All plant tissue culture was performed on Regeneration Media of Plants (RMOP) as described (Svab & Maliga, 1993) and the plants grown in growth cabinets (25°C, 200 ± 50 μmol photons.m^2 illumination, 14:10h L:D) under elevated CO_2 (air + 2%[v/v] CO_2). The tobRr$^{\Delta B2}$ and tob$^{\Delta B2}$ genotypes were grown to maturity in soil in 3 x 2 x 4 meter (L x W x H) controlled environment growth chambers (25°C, 400 ± 100 μmol photons.m^2, 14:10h L:D) under elevated CO_2 (air + 1.5%[v/v] CO_2). For growth comparisons three to six individuals of each genotype were grown. Measurements of plant height (distance from soil to apical

meristem) over time during exponential growth were made until at 72 ± 3 cm in height when samples (0.5 cm^2 discs) from the fifth upper canopy leaf (see Fig 1A) were frozen in N_2 and stored at -80°C. Total above ground dry biomass (including the separate mass of each leaf after measuring their area) were determined after drying at 80°C for 4 days.

Transient BSD2 expression analyses in tob$^{\Delta B2}$*b1* were performed in plants grown under elevated CO_2. The synthetic tobacco, Arabidopsis and maize *bsd2* genes tested (codon modified to avoid tobacco RNAi-*bsd2* silencing) were cloned into the pBIN121 binary vector (Jefferson, 1987) and transformed into *A. tumefaciens* strain GV3101 pMp90. Plants of tob$^{\Delta B2}$*b1* were grown within a growth chamber at 25 °C in air containing 1.5% (v/v) CO_2 until plants reached 15-20 cm in height. Overnight grown (28°C) GV3101 cultures were centrifuged (8000*g,* 1 min), the cell pellets washed in infiltration buffer (10mM MES, 10mM $MgCl_2$ pH5.6) and re-centrifuged before suspending to an OD_{600nm} of 1 in infiltration buffer containing 200 μM acetosyringone (Sigma Aldrich). The cells were infiltrated by 1 mL syringe into the abaxial side of upper canopy leaves. Leaf samples (0.5 cm^2 discs) were harvested 5 days post infiltration, frozen in N_2 and stored at -80°C.

Glasshouse growth comparisons between ten wild type tobacco (control) and ten T_1 tobB2 plants grown in 10 L pots of soil (to avoid becoming root bound) were performed at 20/15°C or 35/30°C (day/night; ± 2°C) under natural illumination. Plants were watered and fertilised using Hoagland's solution every 4 days. At 75 cm in height samples of the upper canopy leaf #5 (see Fig 1A) were frozen in N_2 and stored at -80°C for Rubisco and protein analysis.

Field comparisons of wild type tobacco and tobB2-1 growth and leaf CO_2-assimilation rates were performed on the Energy Farm, at the University of Illinois, Urbana, IL, USA, during June-July 2016. This was fully randomized block design. This consisted of four blocks of 4 x 4 plants for each genotype, surrounded by one border row of wildtype plants. The space between plants was 30 cm, and between blocks 75 cm. Seeds were sown and germinated, and the seedlings were transplanted to trays and to the field as described previously (Kromdijk, Głowacka, Leonelli, Gabilly, Iwai, Niyogi & Long, 2016). The response of leaf CO_2-assimilation rates (A) to intracellular CO_2 concentration (C_i) was measured in three plants per block. Five portable open path gas-exchange systems (LI-6400XT; LI-COR, Inc., Lincoln, NE USA with a LI-6400-40 integrated gas-exchange and modulated chlorophyll fluorescence measuring head) were used to measure the 5th and fully expanded leaf from the apex, 20 days after transplanting. In the leaf cuvettes, photon flux (Q) was set to 2000 μmol m^2 s^{-1}, block temperature to 25 °C, [CO_2] in the sample cell to 400 ppm and leaf-to-air water vapor pressure deficit maintained at <1.5 kPa. Light was provided by the integrated red (635 nm wavelength) and blue (465 nm wavelength) light-emitting diodes (LED), with 10% blue, and 90% red light. A-C_i responses were obtained as described (Long & Bernacchi, 2003). After 30 days in the field, the height of each plant was measured then the above ground biomass determined after drying the stem and leaves separately at 60°C.

Plant BSD2 expression, purification and mass spectrometry.

Recombinant tobacco, potato, Arabidopsis and canola BSD2 were expressed and purified from *E. coli* BL21(DE3) as 6xHistidine tagged ubiquitin (H_6Ub) N-terminal fusion proteins (Fig S1). The purified BSD2 (following H_6Ub removal) was dialysed against 100 mM

ammonium acetate buffer (pH 7.2) and positive ion nanoESI mass spectra acquired using a Waters (Manchester, UK) Synapt^{TM} HDMS^{TM} fitted with a Z-spray nanoESI source (see Fig S2) (Blayney, Whitney & Beck, 2011, Whitney *et al.*, 2015).

Leaf protein and Rubisco extraction, concentration quantification and PAGE.

Leaf proteins were extracted in ice cold extraction buffer (50mM EPPS pH8, 5mM $MgCl_2$ 0.5mM EDTA, 2% (w/v) PVPP, 5% (v/v) glycerol, 1% (v/v/) plant proteinase inhibitor (Sigma), 5mM dithiothreitol) using 2 mL Wheaton glass homogeniser. After centrifugation (16,000*g*, 0.5 to 2 min, 4°C) the soluble protein was collected and aliquots used to quantify Rubisco content by [^{14}C]-2-CABP binding and Rubisco activation status using an enzyme coupled spectrophotometric assay as described (Sharwood, Sonawane, Ghannoum & Whitney, 2016). Protein was measured against BSA using the Pierce Coomassie Protein Assay kit (Thermo Scientific). Protein samples were separated by SDS PAGE (4-12% Bis-Tris SDS-PAGE gels, Invitrogen) or non-denaturing (native) PAGE (4-12% Tris-glycine gels, Invitrogen) as described (Whitney & Sharwood, 2007). The PAGE separated proteins were visualised using Coomassie Blue staining (Thermo Scientific) or blotted onto nitrocellulose membranes and probed with rabbit polyclonal antisera to purified tobacco Rubisco, *R. rubrum* Rubisco or tobacco *Nt*BSD2 (Fig S1). The immunoblots were incubated with enzyme labelled anti-rabbit secondary antibodies and the signals detected using Attophos (Bio-Rad, alkaline phosphatase) or Clarity ECL Blotting Substrate (Bio-Rad, horseradish peroxidase) and visualised using a Bio-Rad VersaDoc system.

Size exclusion chromatography.

Soluble leaf protein extracted from 2 to 4 cm^2 of leaf per mL of ice cold extraction buffer was centrifuged 20,000g at 4°C for 10 min and passed through a 0.22μm filter before loading 0.2 mL onto a Superdex 200 Increase 10/500 GL size exclusion column (GE Healthcare) equilibrated with column buffer (50mM EPPS pH8, 50mM NaCl, 5% [v/v] glycerol). Aliquots of the collected fractions (1 mL) were separated by PAGE and their Rubisco and *Nt*BSD2 content visualised by immunoblotting.

Nucleotide extraction and analysis

Total leaf genomic DNA was isolated using the DNeasy Plant Mini Kit (Qiagen) and used for Southern blotting (Fig S7), PCR amplification and sequencing of transformed plastome regions. Total leaf RNA was purified using the RNeasy Plant Mini Kit (Qiagen) and used for qRT-PCR analysis of *bsd2* mRNA levels in the tobRr (control) and transformed tobRr$^{\Delta BSD2}$ lines (Fig S3B).

Microscopy

Samples for transmission electron microscopy (TEM) were prepared as described previously (Hyman & Jarvis, 2011) with the exception that tertiary fixation with uranyl acetate was omitted. Ultrathin 70 nm sections were made using the Leica EM UC7 Ultramicrotome and then examined using a Hitachi HA7 100 TEM at 100v.

Results

Leaf *Nt*BSD2 content decreases with age

RNAseq information for *N. tabacum* (cv Petite havana) leaves (courteously provided by Dr Maxim Kapralov) identified a prominent *bsd2* transcript which corresponded to NCBI reference sequence XM_016605135. The BSD2 product coded an 81 amino acid mature peptide (8.4 kDa) and a predicted 52 amino acid N-terminal chloroplast targeted transit peptide (Fig. S1A). Antibodies to recombinant *Nt*BSD2 expressed and purified from *Escherichia coli* (Fig. S1B,C) were raised in rabbits and used to quantify its expression in leaves down the canopy of glasshouse grown tobacco during exponential growth (Fig. 1A). *Nt*BSD2-immunoblot analysis of soluble leaf protein against a titration series of purified recombinant *Nt*BSD2 (Fig. 1B) found the amount of cellular *Nt*BSD2 gradually declined from ~70 to 20 nmol protomer.m^2 with leaf age (Fig. 1C, open circles). The leaf Rubisco content showed a similar pattern of decline down the canopy (from ~2.3 to 1.1 μmol L_8S_8 complexes.m^2; Fig 1C, black circles). Accordingly the Rubisco to *Nt*BSD2 molar ratio remained relatively constant with leaf age, particularly in the mature, fully expanded leaves (#5 to #11) where for every *Nt*BSD2 molecule there are 40 to 50 L_8S_8 Rubisco complexes (Figure 1C, blue symbols).

BSDS is associated with Rubisco *in vivo.*

Existing evidence shows the nuclear encoded, cytosol made BSD2 is critical for Rubisco production in plant chloroplasts (including tobacco, (Wostrikoff & Stern, 2007), Figure 2A) and that stable recombinant Arabidopsis Rubisco L_8-BSD2 intermediary complexes of

slightly higher mass than L_8S_8 Rubisco holoenzyme are produced in *E. coli* when S-subunit supply is limiting or absent (Aigner *et al.*, 2017). *Nt*BSD2-immunoblot analyses were undertaken to test whether these intermediary complexes also formed in leaves. Following separation of soluble protein from young upper canopy tobacco leaves (e.g. leaf #5, Figure 1A) by native PAGE a faint band of slightly larger molecular mass than the more diffuse L_8S_8 Rubisco was identified by the *Nt*BSD2 antibody (Figure 2B). This protein complex was annotated L_8(S?)-BSD2 (see below for detail) and was not identified in soluble leaf protein from tobRr leaves - a tobacco genotype where the native L_8S_8 Rubisco is replaced with *R. rubrum* L_2 Rubisco (Figure 2A). Immunoblots using tobacco Rubisco antibody identified the abundant 520 kDa L_8S_8 complex in tobacco (where the amount of WT protein loaded was reduced 20-fold to avoid signal saturation), but not the 100 kDa *R. rubrum* Rubisco (Figure 2B) as its L-subunit shares only 30% sequence identity with the tobacco L-subunit (Whitney & Andrews, 2001).

Size exclusion chromatography (SEC) of recombinant *Nt*BSD2 purified from *E. coli* (Fig S1C) showed it resolved as a low molecular weight product eluting at ~17.5 mL (Figure 2C, grey dashed line). Likewise recombinant BSD2 from potato (*St*BSD2), canola (*Bn*BSD2) and Arabidopsis (*At*BSD2) that were abundantly expressed and purified from *E. coli* (Figure S2D) separated through SEC as comparable sized products to *Nt*BSD2 (Figure S2E). The oligomeric status of each plant BSD2 isoform was examined by electrospray ionisation mass spectrometry (Figure S2). Under non-denaturing conditions all BSD2 proteins were primarily monomeric, with trace amounts of dimer, trimer, tetramer, pentamer and hexamer forms

detected, matching the findings of Aigner *et al.*, (2017). These results indicate the low molecular weight SEC separated BSD2 protein in Figure 2C is un-complexed monomer.

The stable association of *Nt*BSD2 protomers with the large >500 kDa protein complex identified in tobacco leaf protein by native PAGE (Figure 2B) was confirmed using SEC. A prominent L_8S_8 Rubisco peak in the SEC separated tobacco leaf protein was detected at A_{280} (Figure 2C) which matched the Rubisco-immunoblot elution profile (Figure 2D). *Nt*BSD2-immunoblot analysis of the fractions showed an *Nt*BSD2 peak eluting earlier (fraction 3, shaded grey in Fig 2C) than the L_8S_8 peak (fraction 4), consistent with it comprising a structurally stable Rubisco-*Nt*BSD2 intermediary complex. Based on the findings of Aigner et al., (2017) where stable asymmetrical L_8-*Nt*BSD2 complexes comprising some S-subunits can form, this complex was annotated L_8(S?)-BSD2 as the possibility it contains bound S-subunits in addition to *Nt*BSD2 cannot be discounted (Figure 2C). A near equally abundant *Nt*BSD2 peak also eluted in fractions 10-11 of the tobacco sample that matched the elution point of the purified *Nt*BSD2 monomer (Figure 2D). Taken together, the native PAGE (Fig 2B) and SEC (Fig 2D) immunoblot data indicate approximately 50% of the *Nt*BSD2 present in young near fully expanded tobacco leaves is incorporated into proposed L_8(S?)-BSD2 complexes with the remainder present as un-complexed *Nt*BSD2 monomers. If one assumes near stoichiometric *Nt*BSD2 binding in the L_8(S?)-BSD2 complexes (*i.e.* 8 *Nt*BSD2 bound per L_8 core) then they account for <0.2% of the L_8S_8 pool in leaf #5 (*i.e.* 5 nmol $L_8(BSD2)_8.m^2$ relative to 2500 nmol $L_8S_8.m^2$).

Comparative SEC analysis of Rubisco and *Nt*BSD2 production in tobRr leaf protein showed no L_8S_8 Rubisco or L_8(S?)-BSD2 was produced, only *R. rubrum* L_2 Rubisco

(fractions 6 and 7, Figure 2C, E) and un-complexed *Nt*BSD2 (factions 10-11, Fig 2E). This finding supports the assertions that the folding and assembly of *R. rubrum* L_2 Rubisco do not require *Nt*BSD2 and that the >500 kDa *Nt*BSD2 bound protein complex comprises tobacco Rubisco subunits.

The only critical function of BSD2 is in Rubisco biogenesis.

The detection of un-complexed *Nt*BSD2 in tobacco and tobRr leaves questions whether *Nt*BSD2 may serve an additional cellular function in addition to its critical role as a L_8S_8 Rubisco assembly chaperone. To test this two binary vectors targeting RNAi silencing of tobacco *bsd2* mRNA were generated (Figure 3A and S3A) and transformed by Agrobacterium into the nucleus of tobRr which does not require *Nt*BSD2 (or the tobacco S-subunit) for assembly of the foreign L_2 Rubisco (Figure 3B). Reductions in the *bsd2* mRNA levels were confirmed by qRT-PCR in five of the 20 kanamycin resistant tobRr$^{\Delta B2}$*k* plantlets and four of the 15 basta resistant tobRr$^{\Delta B2}$*b* plants tested (Figure S3B). Segregation analyses were performed on 3 lines producing reduced levels of *bsd2* mRNA (tobRr$^{\Delta B2}$*-k1, -k2 and –b1*) to identify homozygous T_1 and T_2 progeny and confirm each contained single transgene insertions (Figure S4). The growth and phenotype of the homozygous T_2 progeny matched the parental tobRr plants (Figure 3C) with *Nt*BSD2-immunoblot analysis of SDS PAGE separated protein unable to detect any *Nt*BSD2 in the leaves of tobRr$^{\Delta B2}$*-k1*, *-k2* or *-b1* plants (Figure 3D). Consistent with their equivalent growth rates and phenotype, the leaf L_2 Rubisco content (Figure 3E) and harvested above ground dry biomass (Figure 3F) in the tobRr$^{\Delta B2}$*-k1, -k2 and -b1* plants matched the parental tobRr plants. Silencing *Nt*BSD2 production also had no distinguishable influence on leaf ultrastructure compared with the tobRr controls (Figure

3G). TEM imaging showed all genotypes contained analogous sized and lens-shaped chloroplasts with comparably organised stromal thylakoid lamellae and grana stacks (Figure S6).

The efficiency of *Nt*BSD2 silencing by RNAi-*bsd2* in the homozygous T_2 tobRr$^{\Delta B2}$-*k1, -k2 and -b1* plants was further evaluated by fertilising wildtype tobacco flowers with their pollen (Fig 4A). The corresponding F_1 progeny (denoted tob$^{\Delta B2}$ and heterozygous for the RNAi-*bsd2* allele) all produced pale green plants with fragile (*i.e.* easily damaged) leaves and their growth was dramatically impaired. In air (0.04% [v/v] CO_2) the growth of the tob$^{\Delta B2}$*k1* and tob$^{\Delta B2}$*k2* lines were particularly encumbered with all plants unable to survive past juvenile growth (Figure 4B). Like their tobRr$^{\Delta B2}$-*k1* and -*k2* parental genotypes the tob$^{\Delta B2}$-*k1* and -*k2* lines produced no detectable *Nt*BSD2 (Figure S5A) and thus very little Rubisco (<0.2 μmol catalytic sites.m^2, Figure 4C). The consequential impairment to photosynthetic carbon assimilation and growth meant that after 11 weeks the tob$^{\Delta B2}$-*k1* and -*k2* plants were still in a juvenile growth stage (Figure 4B) and unable to reach maturity unless grown in elevated CO_2 (Figure S5B). By comparison the tob$^{\Delta B2}$*b1* leaves were able to produce slightly more Rubisco (~1.0 ± 0.3 μmol catalytic sites.m^2) which was >25-fold less than the Rubisco content in wildtype tobacco (Figure 4C). Accordingly, the tob$^{\Delta B2}$-*b1* plants grew substantially slower than wild-type tobacco but faster than the tob$^{\Delta B2}$-*k1* and -*k2* plants in air (Figure 4B) and under elevated CO_2 (Figure S5B). TEM ultrastructure analysis of chloroplasts from elevated CO_2 grown tob$^{\Delta B2}$-*k1* and *b1* leaves showed the Rubisco depleted physiology led to reductions in thylakoid distribution and stacking into grana relative to wildtype (Figure 4D).

Taken together, the contrasting effect of silencing *Nt*BSD2 production on Rubisco production, plant growth and chloroplast ultrastructure between the tobRr$^{\Delta B2}$ lines (no effect detected, Figure 3) and tob$^{\Delta B2}$ lines (all components impaired, Figure 4) indicate the only critical function of *Nt*BSD2 in tobacco is its chaperone role in L_8S_8 Rubisco biogenesis.

The BSD2 chaperone function shows broad plant L-subunit specificity.

Different plant BSD2 isoforms were transiently expressed in the *Nt*BSD2 deficient tob$^{\Delta B2}$-*b1* genotype to compare their capacity to stimulate tobacco L_8S_8 Rubisco biogenesis. Synthetic *bsd2* genes coding the full length BSD2 (including their N-terminal transit peptide (TP) sequence, Figure S1A) from Arabidopsis (*At*BSD2) Zea mays (*Zm*BSD2) and tobacco (*Nt*BSD2, including a control lacking the TP sequence) were cloned into the pBIN121 binary vector and transformed into *Agrobacterium tumefaciens* strain GV3101 (Figure 5A). The codon use of the *bsd2* genes was modified to preclude silencing by the RNAi-*bsd2* allele. The transformed *A. tumefaciens* were infiltrated into the abaxial side of the tob$^{\Delta B2}$-*b1* leaves and samples taken after 5 days. The leaves expressing *At*BSD2, *Zm*BSD2 or *Nt*BSD2 showed 2.5 to 3-fold increases in Rubisco production while those infiltrated with the empty vector or TP lacking *Nt*BSD2 controls showed no change in Rubisco content relative to non-infiltrated leaves (Figure 5B). These findings provide supporting evidence for the chloroplast localized chaperone role of BSD2 in Rubisco biogenesis. These findings also show that the 31% and 33% sequence divergence by *At*BSD2 and *Zm*BSD2 relative to *Nt*BSD2 (Fig S1A) had little, or no, influence on their capacity to stimulate tobacco Rubisco biogenesis. This suggests Rubisco biogenesis may not be extensively biased by sequence complementarity

requirements between BSD2 and its L-subunit substrate, contrary to that observed for the Rubisco specific assembly chaperone Raf1 (Whitney *et al.*, 2015).

Overexpression of *Nt*BSD2 does not affect plant growth, Rubisco content or activation status.

Transplastomic tobacco producing a chloroplast made full length *Nt*BSD2 were generated to test if Rubisco biogenesis and plant growth may be limited by *Nt*BSD2 availability. The synthetic *bsd2* gene from the pNtBSD2 transient expression plasmid (Figure 5A) that is codon optimised to match *rbc*L was transformed into the inverted repeat regions of the chloroplast under the control of the *psbA* regulatory elements (Figure 6A). The resulting tobB2 plants produced both cytosol made (endogenous) and recombinant chloroplast made *Nt*BSD2 that resolved as the same size by SDS PAGE indicating the transit peptide of the transplastomic product was correctly cleavage (Figure 6B). Two of the six independent tobB2 lines produced were regenerated in tissue culture until homoplasmic (Figure S7) then grown to reproductive maturity in soil. Analysis of leaf protein in the T_1 tobB2 progeny (equivalent to leaf #5, Figure 1A) showed they produced approximately 10-fold more *Nt*BSD2 than wildtype tobacco (Figure 6C). SEC analysis of the tobacco and tobB2-1 soluble leaf proteins showed matching A_{280} profiles, including the prominent Rubisco peak (Figure 6D). BSD2-immunoblot analysis of the SEC fractions detected equivalent amounts of L_8(S?)-BSD2 intermediary complexes (Fractions 3 and 4, Figure 6E) in both genotypes and >10-fold more un-complexed *Nt*BSD2 in tobB2-1 (fractions 10-11, Figure 6E). These biochemical analyses suggest that overexpression of *Nt*BSD2 had little, or no, influence on the production of intermediary L_8(S?)-BSD2 complexes or L_8S_8 Rubisco holoenzyme.

The hypothesis that *Nt*BSD2 production is non-limiting to tobacco photosynthesis and growth was supported in glasshouse growth experiments performed in parallel at 20°C (15°C night) and 35°C (30°C night) under natural illumination. At both growth temperatures the wildtype tobacco (control), tobB2-1 or tobB2-2 plants showed no significant difference in growth rate (measured as increase in height over time, Fig 7A), above ground biomass (Fig 7B) or averaged leaf mass area of their entire canopies (LMA, Fig 7C). Similarly there was no variation in the soluble protein, Rubisco content and proportion of active Rubisco in the newest fully expanded leaf (leaf #5, Fig 1A) between each tobacco genotype at 20°C and at 35°C (Fig 7D). Significant variation was observed in the biomass and leaf biochemistry between the growth temperatures. Plants grown at 20°C had a an ~30% enhanced dry biomass (Fig 7B), a ~40% increase in LMA (Fig 7C) and 25% higher leaf soluble protein content (averaging 10.0 ± 0.5 $g.m^2$ across all genotypes) relative to the 35°C grown plants (8.0 ± 0.4 g $protein.m^2$, Fig 7D). The ~20% increase in leaf Rubisco content between the 20°C (averaging 27.7 ± 0.1 μmol catalytic $site.m^2$; ≈1.86 ± 0.06 g $L_8S_8.m^2$) and 35°C (averaging 33.0 ± 0.4 μmol catalytic $site.m^2$; ≈2.21 ± 0.03 g $L_8S_8.m^2$) grown plants only partially accounted for the temperature dependent protein difference (Fig 7D). By contrast the growth temperature and genotype had no significant effect on Rubisco activation with >90% of the enzyme primed for catalysis in all the leaves sampled (Fig 7D, circular symbols, right axis).

A further growth trial in the field under un-regulated temperature, natural illumination and ample fertilizer also showed no significant variation in the growth of tobacco and tobB2-1 plants. Leaf gas exchange measures of photosynthetic rates (*A*) under varying intercellular

CO_2 (C_i) found the *A-Ci* response for both tobacco genotypes were superimposable (Fig 7E). Accordingly there was no significant difference in plant height or above ground biomass between either genotype at the time of harvest (Fig 7F). Taken together the glasshouse and field experiments indicate tobacco Rubisco biogenesis, and hence plant growth, under a range of environmental conditions, including temperature extremes, are not limited by *Nt*BSD2 availability.

Discussion

Following the historic discovery that plant Rubisco assembly requires chaperonin mediated L-subunit folding (Barraclough & Ellis, 1980) it became evident that additional specialised ancillary components were needed in the biogenesis of eukaryotic Rubisco (Roy & Andrews, 2000). This was most apparent following the realisation that the assembly requirements of plant and algae L_8S_8 Rubisco cannot be met by the *E. coli* GroEL-GroES chaperonin complex and associated molecular machinery (Sharwood, 2017, Whitney *et al.*, 2001). Indeed the *E. coli* protein folding components only partly meet the biogenesis needs of many, but not all, bacterial L_8S_8 Rubisco isoforms (Emlyn-Jones *et al.*, 2006, van der Vies, Bradley & Gatenby, 1986, Wilson & Whitney, 2017). Only recently has the expansive cocktail of ancillary proteins required for plant Rubisco bioengineering in *E. coli* finally been resolved (Aigner *et al.*, 2017). The components included subunits of the chloroplast chaperonin folding complex (CPN60α, CPN60β, CPN20) and the assembly chaperones BSD2, Raf1 and Raf2 with the inclusion of RbcX needed to enhance Rubisco yield (Conlan & Whitney, 2018, Wilson & Hayer-Hartl, 2018). This success stemmed from a continuum of structural studies over the last decade that examined the mechanisms of Raf1, RbcX and BSD2 in the assembly and stabilisation of intermediary L_2- to L_8-associated complexes (Bracher *et al.*, 2017). These structural studies utilised *E. coli* expression and *in-vitro* reconstitution methods which necessitated the use of assembly viable cyanobacteria Rubisco L-subunits and, in most cases, heterologous sourced chaperones to enable the formation of stable L_8-chaperone complexes. Attempts to date to identify evidence for the production of L_2/L_8-chaperone intermediary complexes in photosynthetic organisms have been unsuccessful. Here we identify very low

amounts of putative intermediary L_8-Rubisco complexes bound with *Nt*BSD2 that are stably produced in tobacco chloroplasts (Figure 2). In young upper canopy tobacco leaves these L_8-*Nt*BSD2 complexes comprise less than 0.2% of the total L_8S_8 pool, and so have an insignificant impact on measurements of Rubisco content, activity or kinetics using leaf samples.

In accordance with the known requirement for BSD2 in plant Rubisco biogenesis (Aigner *et al.*, 2017, Brutnell *et al.*, 1999, Feiz *et al.*, 2012, Wostrikoff & Stern, 2007) we found *Nt*BSD2 expression varied in tandem with Rubisco content, their amounts highest in the younger, still developing, upper canopy leaves (Figure 1). In the tobRr young upper canopy leaves the pool of monomeric *Nt*BSD2 was ~3-fold lower than wildtype (Figure 3B) consistent with the bacterial L_2 Rubisco produced in this genotype not requiring *Nt*BSD2 (Figure 3A). It would appear that like the unused tobacco S-subunits in tobRr, the redundant *Nt*BSD2 is prone to degradation by stromal proteases.

An ongoing challenge arising from the lethal phenotype associated with deleting BSD2 in plants has been evaluating whether it might play an additional biological function to its critical chaperone role in Rubisco biogenesis (Brutnell *et al.*, 1999, Feiz *et al.*, 2012). As BSD2 exhibits partial structural homology to the translation associated DnaJ chaperone a role for BSD2 in protecting the nascent peptide chain of other chloroplast enzymes can be envisaged (Doron *et al.*, 2014). Our data indicate a chaperone role for BSD2 on non-Rubisco protein substrates is unlikely as silencing *Nt*BSD2 production by RNAi-*bsd2* had no effect on the growth, physiology or cellular ultrastructure in tobRr (Figure 3). Crossing experiments subsequently confirmed the functional specificity of *Nt*BSD2 in L_8S_8 biogenesis whereby the

same RNAi-*bsd2* alleles in wild-type tobacco prevented Rubisco production (Figure 4), which could be reinitiated by re-introducing chloroplast targeted BSD2 isoforms from differing plant sources (Figure 5). We postulate the existence of un-complexed *Nt*BSD2 monomers indicates the inherent levels of this chaperone are non-limiting to Rubisco production in tobacco. In support of this hypothesis the growth, protein and Rubisco biochemistry of the transplastomic tobB2 lines matched wild-type tobacco in the glasshouse and field (Figure 7) despite the >10-fold more *Nt*BSD2 produced in the tobB2 plants (Figure 6).

A role for BSD2 in L-subunit translation in plants remains unclear.

An examination of the BSD2 ortholog in the unicellular algae *Chlamydomonas reinhardtii* (*Cr*BSD2) found it associated with *rbcL* mRNA bound nascent L-subunit peptides suggesting C*r*BSD2 might protect against L-subunit mis-folding (Doron *et al.*, 2014). *Cr*BSD2 additionally showed thiol-reacting activity, an inherent feature of the conserved cysteine rich Zn-finger domain in all BSD2 isoforms (Aigner *et al.*, 2017). It is therefore feasible the reducing activity of BSD2 may prevent premature disulphide bond formation during L-subunit synthesis (Doron *et al.*, 2014). Our finding that silencing *Nt*BSD2 production has no influence on *R. rubrum* L_2 Rubisco biogenesis does not discount either function proposed for *Cr*BSD2. Firstly the assembly of *R. rubrum* Rubisco does not require the formation of disulphide bonds (Schneider, Lindqvist & Lundqvist, 1990), and neither it would appear does Arabidopsis Rubisco (Aigner *et al.*, 2017). Secondly, *R. rubrum* and tobacco Rubisco share <30% sequence identity making it unlikely that *Nt*BSD2 recognises the *R. rubrum* L-subunit. Indeed the simpler L_2-quaternary structure and minimal chaperone requirements of *R. rubrum*

Rubisco are likely what permits its abundant expression in leaf chloroplasts and other heterologous expression hosts (Whitney & Sharwood, 2008). Of note however is in tobRr the *rbcM* gene utilises the endogenous *rbcL* promoter, 5'untranslated region and first 42 nucleotides of *rbcL* coding sequence (also termed the translational control region, TCR (Whitney & Sharwood, 2008)). As *R. rubrum* Rubisco production in tobRr is not compromised by silencing *Nt*BSD2 production it is therefore unlikely any protective function played by *Nt*BSD2 in preventing L-subunit mis-folding involves binding to the highly conserved 14 amino acid N-terminus of plant L-subunits. Nevertheless, we cannot discount the >500 kDa BSD2-macromolecular structure might comprise a BSD2 bound complex associated with L-subunit translation.

Plant Rubisco biogenesis – a S-subunit limited process.

The tobacco L_8-*Nt*BSD2 complexes identified in this study appear highly stable as they are able to maintain unchanged structural confirmation after extended native PAGE electrophoresis and SEC (Figure 2). This finding supports the current model for plant Rubisco biogenesis that has been assembled from multiple Rubisco-chaperone mechanistic studies (Bracher *et al.*, 2017, Wilson & Hayer-Hartl, 2018). The most recent of these studies using Arabidopsis Rubisco has demonstrated the potential for BSD2 to form stable $L_8(BSD2)_8$ intermediary complexes that can be purified and their X-ray structure resolved (Aigner *et al.*, 2017). The process of S-subunit binding and BSD2 displacement from these complexes appears to occur in a co-ordinated manner, even in *E. coli*, where under limiting S-subunit availability the formation of asymmetric L_8-complexes comprising both BSD2 and S-subunits were found to arise (Aigner *et al.*, 2017). It is therefore conceivable the L_8(S?)-

*Nt*BSD2 complex(es) recognised in tobacco leaf protein by the *Nt*BSD2-antibody (Figure 2) may comprise one or more S-subunits. Indeed, transgenic studies to date examining the Rubisco subunit and holoenzyme biochemistry in plants where S-subunit levels have been lowered or increased indicate the rate and amount of Rubisco produced is primarily limited by S-subunit availability (Makino, Nakano, Mae, Shimada & Yamamoto, 2000, Suzuki, Miyamoto, Yoshizawa, Mae & Makino, 2009). Unfortunately the very low abundance and similar size of the L_8(S?)-*Nt*BSD2 complexes relative to L_8S_8 Rubisco (Figure 2) made it unfeasible to ascertain what stoichiometry of S-subunits, if any, were incorporated.

A key limitation in our understanding of Rubisco biogenesis is the process of S-subunit binding and whether it is a chaperone assisted process in plant chloroplasts. The current "S-subunit binding and BSD2 displacement" model assumes mechanistic similarities between plant and cyanobacteria L_8 cores. Indeed, displacement of Arabidopsis BSD2 (*At*BSD2) from heterologous L_8(*At*BSD2)$_8$ complexes (comprising cyanobacteria L-subunits) is readily feasible *in E. coli* when expressed with its cognate cyanobacteria S-subunits. Notably BSD2 is not naturally required in cyanobacteria Rubisco biogenesis, and cyanobacteria S-subunits show rapid, near irreversible binding affinity for their L_8-cores (Andrews & Ballment, 1984). Whether the tobacco S-subunits bind to the L_8-*Nt*BSD2 complexes identified in this study via a comparable independent mechanism or are chaperoned into position to displace bound *Nt*BSD2 remains unclear. A plausible candidate chaperone is Raf2 that has been found via protein cross-linking to have an association with S-subunits in maize (Feiz *et al.*, 2014).

The promiscuous chaperone activity of BSD2 – Rubisco bioengineering considerations.

Prior transplastomic research has demonstrated the requirement for sequence complementarity between plant Rubisco L-subunits and the chaperone Raf1 to augment Rubisco biogenesis (Whitney *et al.*, 2015). Existing evidence shows Raf1 assembles as a dimer to facilitate the formation and stabilisation of L_2Raf1 units (Hauser *et al.*, 2015). These units are joined together and Raf1 apparently displaced via BSD2 binding to form the (more) stable end-state $L_8(BSD2)_8$ complexes – as we identify here in tobacco (Figure 2). Notably the formation of L_2Raf1 units or other Raf1 containing intermediary complexes have not been detected *in planta* (Whitney *et al.*, 2015). This could be due to the pool of available Raf1 in chloroplasts being low. Indeed, the Raf1 levels in young Arabidopsis leaves are ~10 nmol protomer.m^2 (Whitney *et al.*, 2015), approximately 8-fold lower than the *Nt*BSD2 levels in young tobacco leaves (Figure 1). This might explain the inability to detect L-subunit-Raf1 intermediary complexes and raises the question as to whether overexpressing Raf1 might augment Rubisco biogenesis, in particular if Raf1 also provides a stabilising activity to protect L-subunit oligomers from proteolysis (Kolesinski, Rydzy & Szczepaniak, 2017).

Studies with cyanobacteria Rubisco have shown RbcX serves a similar L_2-stabilisation role as Raf1 (Bracher *et al.*, 2017) and for plant Rubisco is important, but not essential, for its assembly in *E. coli* (Aigner *et al.*, 2017). Contrary to Raf1, cyanobacteria Rubisco expression studies in *E. coli* suggest the requirement for sequence complementarity between RbcX and the L-subunits is lessened, somewhat akin to that shown here in the capacity of *At*BSD2, *Zm*BSD2 and *Nt*BSD2 to reinstate tobacco Rubisco biogenesis (Figure

5). This finding, along with the observation the *Nt*BSD2 levels in tobacco are non-limiting to Rubisco biogenesis (Figure 7), suggest that the variation in the amount of heterologous plant L-subunits that can be produced in tobacco chloroplasts (reviewed in (Sharwood, 2017)) unlikely arises from structural incompatibilities with *Nt*BSD2 or the amount of *Nt*BSD2.

LMA, leaf protein and Rubisco content vary with growth temperature.

In an attempt to identify whether *Nt*BSD2 availability may limit Rubisco biogenesis under non-optimal temperatures two glasshouse growth experiments were conducted at 20°C or 35°C. At either temperature extreme the wild-type tobacco and the *Nt*BSD2 over-expressing tobB2 plants showed matching vegetative development and leaf biochemistry. In response to low temperature the plants produced more biomass, correlating with a higher LMA, leaf protein content and amount of Rubisco (Figure 7B to D), closely matching that measured previously for chamber grown tobacco at 20°C and 30°C (Yamori & von Caemmerer, 2009). Somewhat uniquely the adapted glasshouse grown plants had near saturating Rubisco activation levels at both growth temperatures (Fig 7D). This finding is in stark contrast to transitory temperature response analyses where C_3-plants like tobacco, wheat and cotton grown at 25 to 28°C show a decline in Rubisco activation status when the temperature is increased (Crafts-Brandner & Salvucci, 2000, Feller, Crafts-Brandner & Salvucci, 1998, Yamori, Evans & Von Caemmerer, 2010, Yamori & von Caemmerer, 2009). This activity decline is attributed (primarily) as a response to reductions in Rubisco activase activity arising from thermally induced denaturation and aggregation (Crafts-Brandner & Salvucci, 2000, Feller *et al.*, 1998). Understanding the mechanism by which near full Rubisco

activation can acclimate in tobacco grown under continuous low and high temperature extremes remains to be fully appraised.

Conclusion

The need to feed and fuel a growing global population has led to increased exploitation of modern synthetic biology tools (SynBio) to adjust photosynthetic metabolism for enhancement of plant growth (Long *et al.*, 2015). Alternative foci are exploring the potential of novel SynBio CO_2-fixation systems aimed at either complementing or replacing components of photosynthetic carbon fixation in bacteria, algae and, possibly in time, in plants (Erb & Zarzycki, 2018). A consensus shared by all endeavours is that increasing the yield potential of crops will likely require a combination of metabolic changes – either sourced via mining natural diversity or obtained via artificial modification. A key target for kinetic improvement has been Rubisco. We now know it is feasible to improve the kinetics of Archaea Rubisco and Form I cyanobacteria Rubisco (Wilson *et al.*, 2016, Wilson *et al.*, 2018) but emulating this success with plant Rubisco has been hindered by being unable to express and test in *E. coli* or transplant the more efficient red algae Rubisco into plant chloroplasts (Sharwood, 2017). Only through deriving the sequential mechanistic details of the auxiliary protein requirements for plant Rubisco biogenesis did the prized goal of producing recombinant Rubisco in *E. coli* finally become achievable (Aigner *et al.*, 2017). Here we provide evidence that the predicted recombinant BSD2-associated Rubisco end-state assembly intermediate identified using *E. coli* is also naturally produced in leaf chloroplasts. It is also now evident BSD2 availability and its promiscuity as a chaperone will likely not

limit foreign Rubisco biogenesis in plants – even when grown under non-optimal temperatures or under the “real-world” fluctuating temperatures and illumination in the field.

Acknowledgment:

This research was supported by the Australian Government through the Australian Research Council Centre of Excellence for Translational Photosynthesis CE140100015 and LE0882289 (JB) and Bill and Melinda Gates Foundation grant OPP1060461 titled "RIPE - Realizing increased photosynthetic efficiency for sustainable increases in crop yield". We thank David Drag and Ben Harbaugh (University of Illinois) for managing the field site and acknowledge the facilities and technical assistance of the Australian Microscopy & Microanalysis Research Facility at the Centre of Advanced Microscopy, the Australian National University.

References:

Aigner H., Wilson R.H., Bracher A., Calisse L., Bhat J.Y., Hartl F.U. & Hayer-Hartl M. (2017) Plant Rubisco assembly in *E. coli* with five chloroplast chaperones including BSD2. *Science*, **358**, 1272-1278.

Andrews T.J. & Ballment B. (1984) A rapid, sensitive method for quantitating subunits in purified ribulose bisphosphate carboxylase preparations. *Plant Physiology*, **75**, 508-510.

Barraclough R. & Ellis R.J. (1980) Protein synthesis in chloroplasts. IX. Assembly of newly-synthesized large subunits into ribulose bisphosphate carboxylase in isolated intact pea chloroplasts. *Biochim. Biophys. Acta*, **608**, 18-31.

Blayney M., Whitney S. & Beck J. (2011) NanoESI mass spectrometry of Rubisco and Rubisco activase structures and their Interactions with nucleotides and sugar phosphates. *Journal of The American Society for Mass Spectrometry*, **22**, 1588-1601.

Bracher A., Whitney S.M., Hartl F.U. & Hayer-Hartl M. (2017) Biogenesis and metabolic maintenance of Rubisco. *Annual Review of Plant Biology*, **68**, 29-60.

Brutnell T.P., Sawers R.J.H., Mant A. & Langdale J.A. (1999) Bundle sheath defective2, a novel protein required for post-translational regulation of the *rbc*L gene of maize. *Plant Cell*, **11**, 849-864.

Carmo-Silva E., Scales J.C., Madgwick P.J. & Parry M.A.J. (2015) Optimizing Rubisco and its regulation for greater resource use efficiency. *Plant, Cell & Environment*, **38**, 1817-1832.

Conlan B. & Whitney S. (2018) Preparing Rubisco for a tune up. *Nature Plants*, **4**, 12-13.

Crafts-Brandner S.J. & Salvucci M.E. (2000) Rubisco activase constrains the photosynthetic potential of leaves at high temperature and CO2. *Proceedings of the National Academy of Sciences of the United States of America*, **97**, 13430-13435.

Doron L., Segal N., Gibori H. & Shapira M. (2014) The BSD2 ortholog in *Chlamydomonas reinhardtii* is a polysome-associated chaperone that co-migrates on sucrose gradients with the *rbcL* transcript encoding the Rubisco large subunit. *Plant J.*, **80**, 345-355.

Durao P., Aigner H., Nagy P., Mueller-Cajar O., Hartl F.U. & Hayer-Hartl M. (2015) Opposing effects of folding and assembly chaperones on evolvability of Rubisco. *Nat. Chem. Biol.*, **11**, 148-155.

Emlyn-Jones D., Woodger F.J., Price G.D. & Whitney S.M. (2006) RbcX can function as a Rubisco-chaperonin, but is non essential in *Synechococcus* PCC7942. *Plant Cell Physiol.*, **47**, 1630-1640.

Erb T.J. & Zarzycki J. (2018) A short history of RubisCO: the rise and fall (?) of Nature's predominant CO2 fixing enzyme. *Current Opinion in Biotechnology*, **49**, 100-107.

Evans J. & Seemann J. (1989) The allocation of nitrogen in the photosynthetic apparatus: costs, consequences and control. In: *Photosynthesis* (ed W.R. Briggs), pp. 183-205. Alan R Liss, Inc, New York.

Feiz L., Williams-Carrier R., Belcher S., Montano M., Barkan A. & Stern D.B. (2014) A protein with an inactive pterin-4a-carbinolamine dehydratase domain is required for Rubisco biogenesis in plants. *Plant J.*, **80**, 862-869.

Feiz L., Williams-Carrier R., Wostrikoff K., Belcher S., Barkan A. & Stern D.B. (2012) Ribulose-1,5-bis-phosphate carboxylase/oxygenase accumulation factor1 is required for holoenzyme assembly in maize. *Plant Cell*, **24**, 3435-3446.

Feller U., Crafts-Brandner S.J. & Salvucci M.E. (1998) Moderately high temperatures inhibit ribulose-1,5-bisphosphate carboxylase/oxygenase (Rubisco) activase-mediated activation of Rubisco. *Plant Physiology*, **116**, 539-546.

Hauser T., Bhat J.Y., Milicic G., Wendler P., Hartl F.U., Bracher A. & Hayer-Hartl M. (2015) Structure and mechanism of the Rubisco-assembly chaperone Raf1. *Nat. Struct. Mol. Biol.*, **22**, 720-728.

Hyman S. & Jarvis R.P. (2011) Studying Arabidopsis chloroplast structural organisation using transmission electron microscopy. In: *Chloroplast Research in Arabidopsis: Methods and Protocols, Volume I* (ed R.P. Jarvis), pp. 113-132. Humana Press, Totowa, NJ.

Jefferson R.A. (1987) Assaying chimeric genes in plants: The GUS gene fusion system. *Plant Molecular Biology Reporter*, **5**, 387-405.

Kolesinski P., Rydzy M. & Szczepaniak A. (2017) Is RAF1 protein from Synechocystis sp. PCC 6803 really needed in the cyanobacterial Rubisco assembly process? *Photosynthesis Research*, **132**, 135-148.

Kromdijk J., Głowacka K., Leonelli L., Gabilly S.T., Iwai M., Niyogi K.K. & Long S.P. (2016) Improving photosynthesis and crop productivity by accelerating recovery from photoprotection. *Science*, **354**, 857-861.

Lin M.T., Occhialini A., Andralojc P.J., Parry M.A. & Hanson M.R. (2014) A faster Rubisco with potential to increase photosynthesis in crops. *Nature*, **513**, 547-550.

Liu C., Young A.L., Starling-Windhof A., Bracher A., Saschenbrecker S., Rao B.V., Rao K.V., Berninghausen O., Mielke T., Hartl F.U., Beckmann R. & Hayer-Hartl M. (2010) Coupled chaperone action in folding and assembly of hexadecameric Rubisco. *Nature*, **463**, 197-202.

Long B.M., Hee W.Y., Sharwood R.E., Rae B.D., Kaines S., Lim Y.-L., Nguyen N.D., Massey B., Bala S., von Caemmerer S., Badger M.R. & Price G.D. (2018) Carboxysome encapsulation of the CO_2-fixing enzyme Rubisco in tobacco chloroplasts. *Nature Communications*, **9**, 3570.

Long S.P. & Bernacchi C.J. (2003) Gas exchange measurements, what can they tell us about the underlying limitations to photosynthesis? Procedures and sources of error. *Journal of Experimental Botany*, **54**, 2393-2401.

Long Stephen P., Marshall-Colon A. & Zhu X.-G. (2015) Meeting the global food demand of the future by engineering crop photosynthesis and yield potential. *Cell*, **161**, 56-66.

Makino A. (2003) Rubisco and nitrogen relationships in rice: Leaf photosynthesis and plant growth. *Soil Science and Plant Nutrition*, **49**, 319-327.

Makino A., Nakano H., Mae T., Shimada T. & Yamamoto N. (2000) Photosynthesis, plant growth and N allocation in transgenic rice plants with decreased Rubisco under CO2 enrichment. *Journal of Experimental Botany*, **51**, 383-389.

Mueller-Cajar O. & Whitney S.M. (2008) Directing the evolution of Rubisco and Rubisco activase: first impressions of a new tool for photosynthesis research. *Photosynthesis Research*, **98**, 667-675.

Oh T.R., Kim J.H., Cho S.K., Ryu M.Y., Yang S.W. & Kim W.T. (2017) AtAIRP2 E3 ligase affects ABA and high-salinity responses by stimulating its ATP1/SDIRIP1 substrate turnover. *Plant Physiology*, **174**, 2515-2531.

Rikard F., Chen H., Nicole W., M. R.L., M. W.R., Linda S., Jeremy H., M. K.D., S. M.S., Todd Y. & Roberta C. (2018) RAF2 is a RuBisCO assembly factor in *Arabidopsis thaliana*. *The Plant Journal*, **94**, 146-156.

Roy H. & Andrews T.J. (2000) Rubisco: Assembly and Mechanism. In: *Photosynthesis: Physiology and Metabolism* (eds R.C. Leegood, T.D. Sharkey, & S. von Caemmerer), pp. 53-83. Kluwer Academic Publishers, Dordrecht.

Salesse C., Sharwood R., Sakamoto W. & Stern D. (2017) The Rubisco chaperone BSD2 may regulate chloroplast coverage in maize bundle sheath cells. *Plant Physiology*, **175**, 1624-1633.

Schneider G., Lindqvist Y. & Lundqvist T. (1990) Crystallographic refinement and structure of ribulose-1,5-bisphosphate carboxylase from *Rhodospirillum rubrum* at 1.7 Å resolution. *Journal of Molecular Biology*, **211**, 989-1008.

Sharwood R.E. (2017) Engineering chloroplasts to improve Rubisco catalysis: prospects for translating improvements into food and fiber crops. *New Phytologist*, **213**, 494-510.

Sharwood R.E., Ghannoum O., Kapralov M.V., Gunn L.H. & Whitney S.M. (2016) Temperature responses of Rubisco from Paniceae grasses provide opportunities for improving C_3 photosynthesis. *Nature Plants*, **2**, 16186.

Sharwood R.E., Sonawane B.V., Ghannoum O. & Whitney S.M. (2016) Improved analysis of C_4 and C_3 photosynthesis via refined *in vitro* assays of their carbon fixation biochemistry. *Journal of Experimental Botany*, **67**, 3137-3148.

Sun Q., Li Y.-Y., Wang Y., Zhao H.-H., Zhao T.-Y., Zhang Z.-Y., Li D.-W., Yu J.-L., Wang X.-B., Zhang Y.-L. & Han C.-G. (2018) Brassica yellows virus P_0 protein impairs the antiviral activity of NbRAF2 in *Nicotiana benthamiana*. *Journal of Experimental Botany*, **69**, 3127-3139.

Suzuki Y., Miyamoto T., Yoshizawa R., Mae T. & Makino A. (2009) Rubisco content and photosynthesis of leaves at different positions in transgenic rice with an overexpression of RBCS. *Plant, Cell & Environment*, **32**, 417-427.

Svab Z. & Maliga P. (1993) High-frequency plastid transformation in tobacco by selection for a chimeric *aadA* gene. *Proceedings of the National Academy of Sciences of the United States of America*, **90**, 913-917.

van der Vies S.M., Bradley D. & Gatenby A.A. (1986) Assembly of cyanobacterial and higher-plant ribulose bisphosphate carboxylase subunits into functional homologous and heterolougous enzyme molecules in escherichia-coli. *EMBO Journal*, **5**, 2439-2444.

Whitney S.M. & Andrews T.J. (2001) Plastome-encoded bacterial ribulose-1,5-bisphosphate carboxylase/oxygenase (Rubisco) supports photosynthesis and growth in tobacco. *Proc Natl Acad Sci*, **98**, 14738-14743.

Whitney S.M., Baldet P., Hudson G.S. & Andrews T.J. (2001) Form I Rubiscos from non-green algae are expressed abundantly but not assembled in tobacco chloroplasts. *Plant Journal*, **26**, 535-547.

Whitney S.M., Birch R., Kelso C., Beck J.L. & Kapralov M.V. (2015) Improving recombinant Rubisco biogenesis, plant photosynthesis and growth by coexpressing its ancillary RAF1 chaperone. *Proc. Natl. Acad. Sci. U S A*, **112**, 3564-3569.

Whitney S.M. & Sharwood R.E. (2007) Linked Rubisco subunits can assemble into functional oligomers without impeding catalytic performance. *Journal of Biological Chemistry*, **282**, 3809-3818.

Whitney S.M. & Sharwood R.E. (2008) Construction of a tobacco master line to improve Rubisco engineering in chloroplasts. *J Exp Bot* **59**, 1909-1921.

Wilson R.H., Alonso H. & Whitney S.M. (2016) Evolving *Methanococcoides burtonii* archaeal Rubisco for improved photosynthesis and plant growth. *Sceintific Reports*, **6**, 22284.

Wilson R.H. & Hayer-Hartl M. (2018) Complex chaperone dependence of Rubisco biogenesis. *Biochemistry*.

Wilson R.H., Martin-Avila E., Conlan C. & Whitney S.M. (2018) An improved *Escherichia coli* screen for Rubisco identifies a protein–protein interface that can enhance CO_2-fixation kinetics. *Journal of Biological Chemistry*, **293**, 18-27.

Wilson R.H. & Whitney S.M. (2017) Improving CO_2 fixation by enhancing Rubisco performance. In: *Directed Enzyme Evolution: Advances and Applications* (ed M. Alcalde), pp. 101-126. Springer International Publishing, Cham.

Wostrikoff K. & Stern D. (2007) Rubisco large-subunit translation is autoregulated in response to its assembly state in tobacco chloroplasts. *Proceedings of the National Academy of Sciences*, **104**, 6466-6471.

Yamori W., Evans J.R. & Von Caemmerer S. (2010) Effects of growth and measurement light intensities on temperature dependence of CO_2 assimilation rate in tobacco leaves. *Plant, Cell & Environment*, **33**, 332-343.

Yamori W. & von Caemmerer S. (2009) Effect of Rubisco Activase Deficiency on the Temperature Response of CO₂ Assimilation Rate and Rubisco Activation State: Insights from Transgenic Tobacco with Reduced Amounts of Rubisco Activase. *Plant Physiology*, **151**, 2073-2082.

Figure legends:

Figure 1. Variation in leaf Rubisco and BSD2 levels within the tobacco canopy.

(A) Example phenotype of a glasshouse grown tobacco 48 days post cotyledon emergence (72 cm in height). Shown are the leaves analysed and their number from the apical meristem. (B) Example immunoblot of soluble protein from 3 mm^2 of leaf material used to quantify leaf tobacco BSD2 (*Nt*BSD2) amounts against a titration series of *E. coli* purified recombinant *Nt*BSD2 (see Fig S1). (C) Variation down the tobacco canopy of leaf Rubisco (L_8S_8) content (left Y-axis), BSD2 content (right Y-axis) and their molar ratio (far right Y-axis, blue). Data is the average (± SD) of comparable leaf samples from 3 tobacco plants.

Figure 2. Detection of putative L_8-BSD2 intermediary complexes in tobacco chloroplasts.

(A) L_8S_8 Rubisco assembly in tobacco (tob) from chloroplast made L-subunits and imported cytosol made S-subunits requires the nuclear encoded chaperone *Nt*BSD2 (Wostrikoff & Stern, 2007). In contrast the S-subunits and *Nt*BSD2 are unnecessary for recombinant L_2 Rubisco production in the transplastomic tobacco genotype tobRr (Whitney & Sharwood, 2008). (B) Native PAGE separated tob and tobRr leaf soluble protein with an NtBSD2-immunoblot that detects a protein complex (labelled L_8(S)-BSD2) migrating slightly slower (*i.e.* larger in size) than L_8S_8 Rubisco in tob. No L_8(S)-BSD2 or L_8S_8 complexes were detected in tobRr using *Nt*BSD2 or tobacco Rubisco-antibodies. (C) Comparative elution profiles of tobacco (black line) and tobRr (blue line) leaf protein and *E. coli* purified NtBSD2 (dotted grey line, see Figure S1E) following Superdex 200 size exclusion chromatography

(SEC). The differing elution peaks for tob L_8S_8 Rubisco (~520 kDa), tobRr L_2 Rubisco (~100 kDa) and *Nt*BSD2 monomer (8.4 kDa) are shown. (D) Immunoblots of the tob fractions show the highest Rubisco content (Rubisco Ab) in fraction 4 and two *Nt*BSD2 peaks (*Nt*BSD2 Ab) in fraction 3 (L_8(S?)-BSD2 intermediary complexes, shaded grey) and fraction 11 (un-complexed *Nt*BSD2). (E) No L_8(S?)-BSD2 intermediary complexes were detected by immunoblot analysis of the tobRr SEC fractions, only un-complexed *Nt*BSD2 (Fraction 11) that elutes after L_2 Rubisco which separates in fractions 6 and 7.

Figure 3. RNAi-silencing of BSD2 production in tobRr does not affect leaf biochemistry or plant growth.

(A) Summary features of the RNAi-*bsd2* nucleus transforming plasmids ptobRNAi-B2*k* (containing *nptII* that codes kanamycin resistance) and ptobRNAi-BSD2*b* (containing *bar* which encodes basta resistance) coding inverted duplicate copies of *bsd2*. CS_{int}, chalcone synthase intron loop; P_{CV}, cauliflower mosaic virus 35S promoter; P_{nos}/T_{nos}, nopaline synthase promoter/terminator sequences; P_{MS}/T_{MS}, mannopine synthase promoter/terminator sequences; see Fig S3A for detail on the RNAi-*bsd2* cassette. (B) The plasmids were Agrobacterium transformed into tobRr and multiple independently transformed tobRr$^{\Delta B2}$*k* and tobRr$^{\Delta B2}$*b* lines obtained that showed varying reductions in *bsd2* mRNA levels (see Fig S3B). Homozygous T_2 tobRr$^{\Delta B2}$*k1*, tobRr$^{\Delta B2}$*k2* and tobRr$^{\Delta B2}$*b1* lines were identified by segregation analysis (Figure S4) whose (C) growth and phenotype matched the tobRr parental control plants after 39 days post-cotyledon emergence (pce) under 450 ± 50 mol photons.m^2.s^{-1} illumination (14h:10h, L:D) at 25°C in air containing 1.5% (v/v) CO_2. (D) Soluble protein from leaf #5 (mm^2 of leaf protein loaded is shown in italics) from each genotype (and wild-

type tobacco, tob) at 45±2 cm in height was separated by SDS PAGE and either Coomassie stained or immunoblotted with *Nt*BSD2 antisera and the amount quantified against a titration series of purified *Nt*BSD2 (see Figure 1B). nd, not detected. (E) Leaf Rubisco content and (F) total above ground plant dry weight of each tobRr derived genotype showed no significant difference. (G) Representative TEM images showing the comparable ultrastructure of chloroplasts from tobRr, tobRr$^{\Delta B2}$*k1* and tobRr$^{\Delta B2}$*b1* (see Figure S6 for more TEM micrographs). Letters indicate the characteristic plastoglobule (p) stromal lamellae (sl) and stacked grana lamellae (grana, g) of chloroplasts.

Figure 4. RNAi-silencing of BSD2 in tobacco impairs L_8S_8 Rubisco biogenesis.

(A) Schematic showing silencing of *Nt*BSD2 production in wildtype tobacco (tob) by introducing RNAi-*bsd2* alleles via fertilising tob (wt) flowers with pollen from homozygous T_2 tobRr$^{\Delta B2}$*k* or tobRr$^{\Delta B2}$*b* to produce heterozygous F_1 tob$^{\Delta B2}$*k* or tob$^{\Delta B2}$*b* progeny that produced very little (tob$^{\Delta B2}$*b1*) or no detectable amounts (tob$^{\Delta B2}$*k1*, tob$^{\Delta B2}$*k2*) of *Nt*BSD2 protein (Figure S5A). (B) The growth of the tob$^{\Delta B2}$*b1* progeny in air was more than 2-fold slower than the tob controls, with tob$^{\Delta B2}$*k1* and tob$^{\Delta B2}$*k2* growth impeded more significantly (even under elevated CO_2, FigS5B). (C) Rubisco content (quantified by ^{14}CABP binding) in young leaves of glasshouse grown plants and (D) TEM images of their chloroplast ultrastructure showing plastoglobule (p) production is preserved while thylakoid prevalence and arrangement as stromal lamellae (sl) and stacked grana lamellae (grana, g) is increasingly more diffuse in the pale green tob$^{\Delta B2}$*b1* and even paler tob$^{\Delta B2}$*k1* leaves (see Figure S6 for additional TEM micrographs).

Figure 5. Transient expression of BSD2 in tob$^{\Delta B2}$*b1* restores L_8S_8 Rubisco biogenesis.

(A) Genes coding *Nt*BSD2 (tob, including non-chloroplast targeting p*Nt*BSD2(ΔTP) control), and BSD2 from Arabidopsis (*At*BSD2) and corn (*Zm*BSD2, see Figure S1 for sequences) were cloned into the pBIN121 binary vector and transiently expressed via Agrobacterium GV3101 infiltration into tob$^{\Delta B2}$*b1* leaves. The genes were codon modified (cm) to avoid similarity with the RNAi-*bsd2* sequence and included their respective N-terminal transit peptide (TP) sequences. The capacity of each chloroplast targeted recombinant BSD2 (depicted by orange ellipse in cartoon schematic) to facilitate tobacco L_8S_8 Rubisco biogenesis was (B) quantified by ^{14}C-CABP binding using samples taken 5 days post Agro-infiltration (dpi) from 3 separately infiltrated leaf regions (±SD). Each recombinant BSD2 stimulated tobacco Rubisco biogenesis to similar extents (black bars) while Rubisco levels remained unchanged in the TP lacking p*Nt*BSD2(ΔTP) and pBIN19 empty vector controls (white bars). Different letters denote a significant difference, whereas the same letters denote no significant difference (two-tailed t-test, $P < 0.05$).

Figure 6. Transplastomic overexpression of BSD2 in tobacco.

(A) The plastome transforming plasmid pRVBSD2 derived from pRV112a (Svab & Maliga, 1993) contained a synthesized tobacco full length *bsd2* gene (i.e. coding its native transit peptide, TP) whose codon use matched *rbc*L. Plastome flanking sequence in pRVBSD2 directed insertion of the *aadA* (spectinomycin selectable marker gene) and *bsd2* transgene into both inverted repeat regions (IR_A/IR_B) of the wildtype tobacco plastome (numbered relative to the IR_A insertion region of the plastome, Genbank Z00044). (B) The resulting

tobB2 transplastomic lines produce both chloroplast made recombinant and native cytosol made *Nt*BSD2 (orange ellipses). (C) Coomassie stain (upper panel) and *Nt*BSD2-immunoblot (lower panel) analyses of SDS PAGE separated soluble protein from 2 mm^2 of comparable young leaves sampled from 45 cm in height, glass house grown tobacco (tob wt) and two independently transformed homoplasmic T_1 tobB2 lines. Shown are the leaf *Nt*BSD2 contents quantified via *Nt*BSD2-immunoblots (see Figure 1B). (D) Size exclusion chromatography (SEC) of soluble protein from 0.4 cm^2 of young tob (black line) and tobB2-1 (blue dashed line) leaves with equivalent Rubisco contents (*i.e.* comparable A_{280} L_8S_8 peaks). (E) *Nt*BSD2 immunoblot analysis of SEC fractions showed the >10-fold elevated *Nt*BSD2 levels in tobB2 accumulated as un-complexed monomers while the content of intermediary L_8(S?)-BSD2 complexes matched wild-type tobacco.

Figure 7. BSD2 overexpression has no effect on the growth, leaf biochemistry or photosynthesis rate of tobacco grown in the glass house or field.

(A) Comparative growth of wild-type tobacco (tob) and T_2 progeny of the *Nt*BSD2 overexpressing tobB2-1 and tobB2-2 transplastomic genotypes grown under natural illumination (Nov-Dec 2016, Canberra, Australia) in temperature controlled glasshouses at either 20 ± 2°C (grey bars) or 35 ± 3°C (white bars). Shown are the increase in average plant height (n = 10 plants per genotype ± SD) over time during exponential growth. The plants in each temperature treatment were simultaneously harvested (plants were 71 ± 4 cm in height) and (B) total above ground dry biomass (stem + leaves) and (C) averaged leaf mass area (LMA) determined after drying at 80°C for 4 d. (D) Prior to harvesting samples from leaf #5 were sampled to quantify soluble protein (left axis), Rubisco content (black/dark grey bars,

left axis) and Rubisco activation status (right axis). No significant differences were observed in the (E) leaf *A-Ci* response of field grown (June-July 2016, Urbana, IL, USA) tob and tobB2-1 plants (n = 4 ± SD) measured at day 20 in the field or in (F) their corresponding height ($p = 0.099$) and above ground dry weights (leaf, white bars; stem, black bars, $p = 0.149$) 30 days after seedling transplantation in the field.

Summary statement

BSD2 is a Rubisco specific assembly chaperone, forms intermediary hetero-oligomeric complexes and is non-limiting to growth in tobacco.

The required sequence complementarity by plant Rubisco for components of its complex biogenesis interactome poses a significant obstacle to improving catalysis. Here we detail evidence the Rubisco chaperone BSD2 forms stable intermediary complexes with Rubisco in tobacco and that BSD2 availability does not limit Rubisco biogenesis, photosynthesis or plant growth in this model C3-plant. We show the only critical role of BSD2 in tobacco is in Rubisco biogenesis and that BSD2 is not species specific and can effectively assemble Rubisco from differing plant species. This work provides a significant advance in engineering photosynthesis and in understanding the folding machinery of chloroplasts and Rubisco.

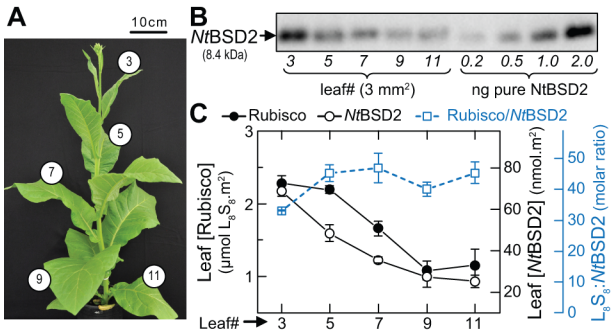

PCE_13473_F1.tif

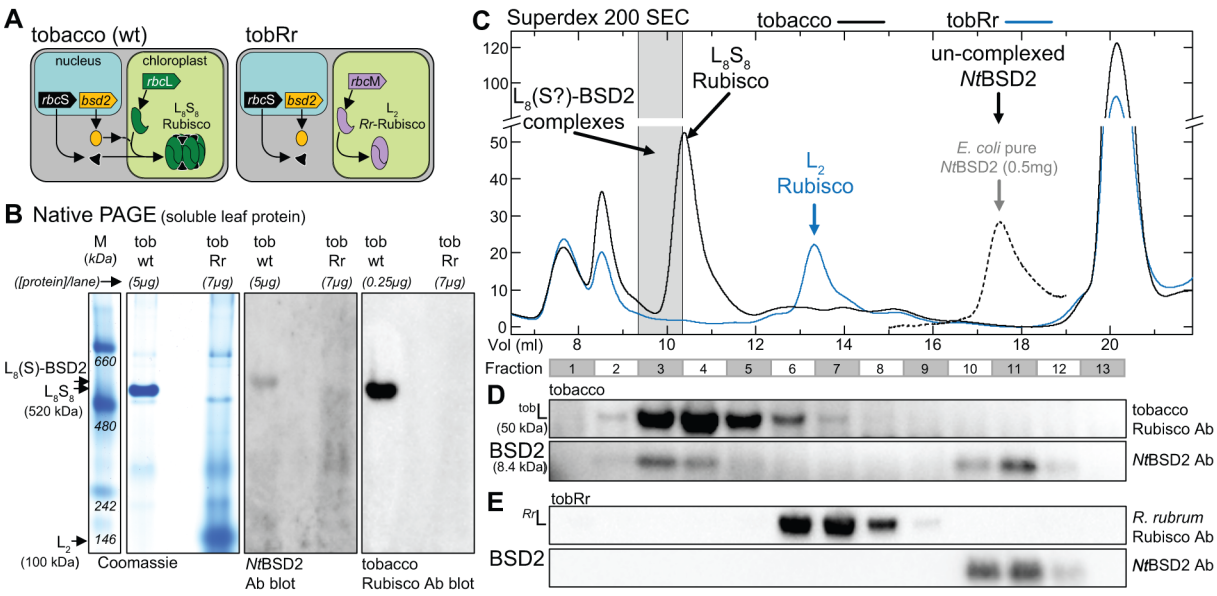

PCE_13473_F2.tif

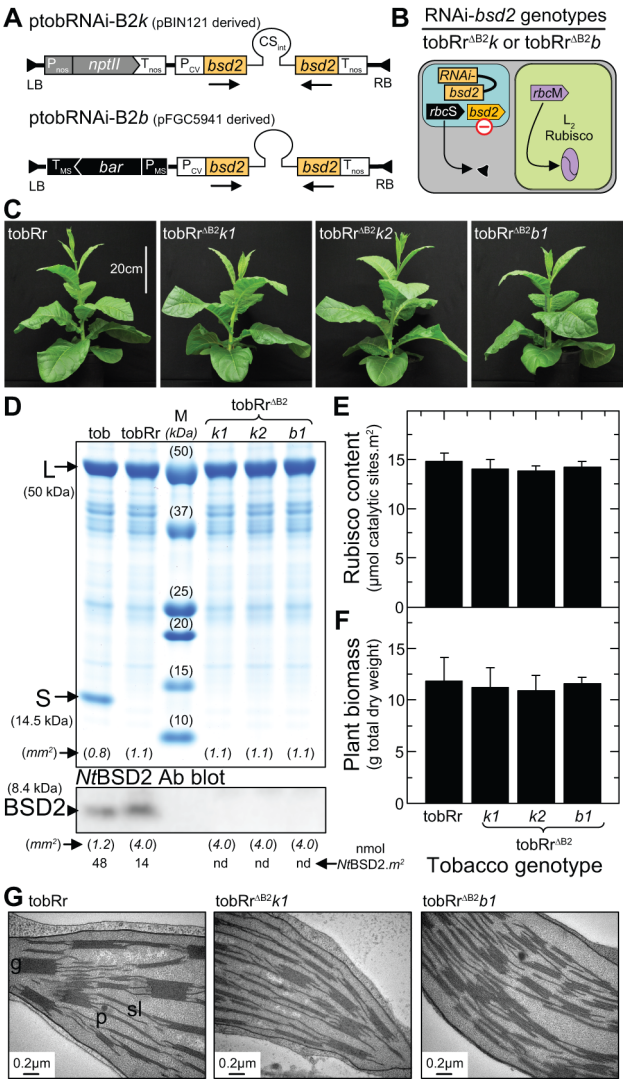

PCE_13473_F3.tif

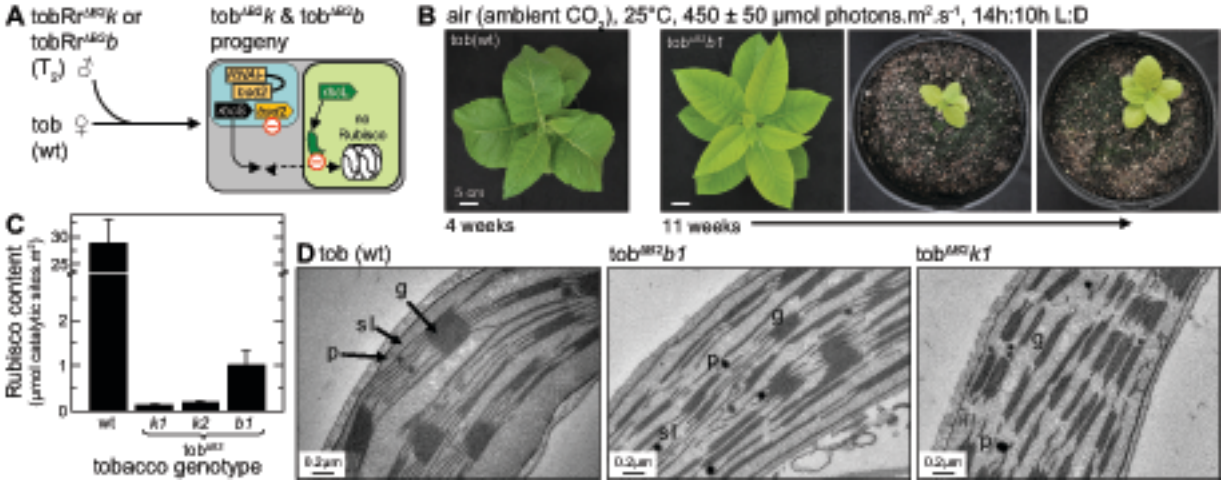

PCE_13473_F4.tif

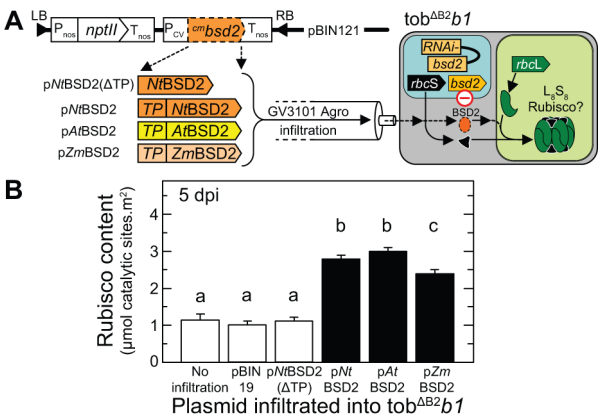

PCE_13473_F5.tif

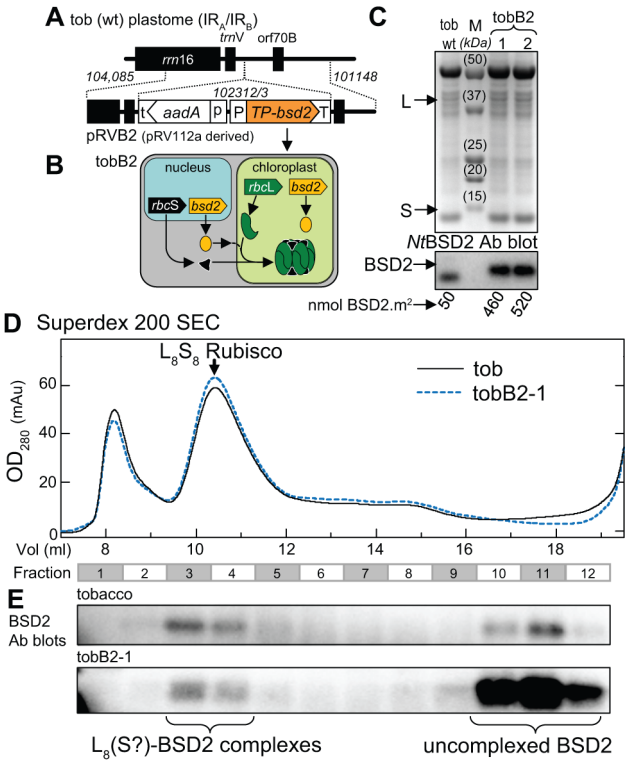

PCE_13473_F6.tif

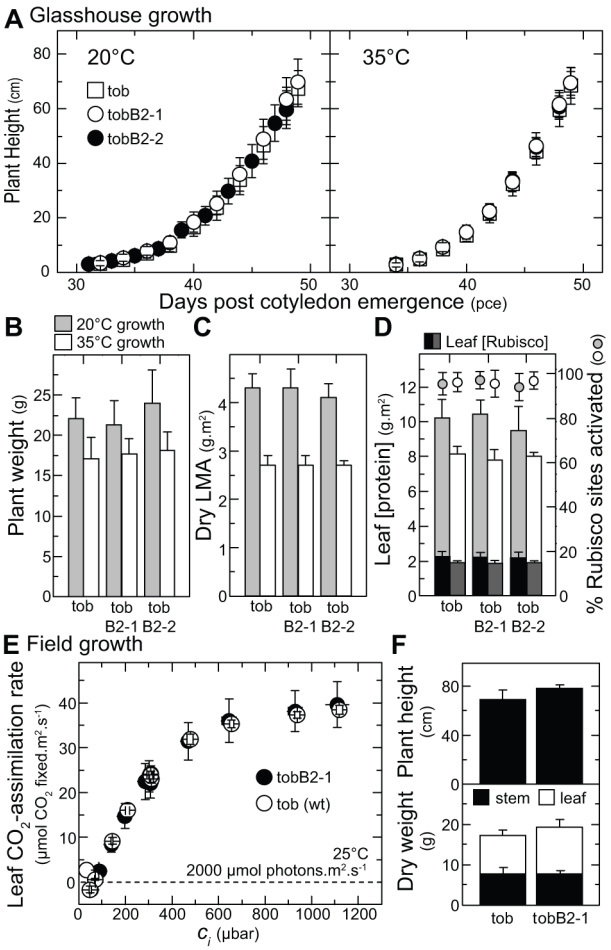

PCE_13473_F7.tif